COMPUTING CONFINED ELASTICAE

SÖREN BARTELS AND PASCAL WEYER

ABSTRACT. A numerical scheme for computing arc-length parametrized curves of low bending energy that are confined to convex domains is devised. The convergence of the discrete formulations to a continuous model and the unconditional stability of an iterative scheme are addressed. Numerical simulations confirm the theoretical results and lead to a classification of observed optimal curves within spheres.

1. INTRODUCTION

Equilibrium configurations of thin elastic rods have been of interest since the times of Euler. The mathematical modelling of these deformable structures has been reduced from three dimensions to a one-dimensional problem for the center-line of the rod $u : I \to \mathbb{R}^3$, cf. [31, 28, 21, 36, 8]. In the bending regime, the rod is inextensible so that $|u'| = 1$ holds on I. Considering a circular cross section and omitting twist contributions, the elastic energy reduces to the functional

$$E_{\text{bend}}[u] = \frac{\kappa}{2} \int_I |u''(x)|^2 \, \mathrm{d}x$$

for a parameter $\kappa > 0$ that describes the bending rigidity. Elasticae, i.e. rods of minimal bending energy, can be stated explicitly e.g. for periodic boundary conditions [33, 32]. Applications of elastic thin rods include DNA modelling [42, 26, 1], the movement of actin filaments in cells [35] or of thin microswimmers [40], the fabrication of textiles [29], and investigating the reach of a rod injected into a cylinder [37].

To obtain minimally bent elastic rods, the bending energy can be reduced by a gradient-flow approach. This method can be used for analytic considerations, cf. for instance [32, 25, 38, 18, 41] and numerical computations [20, 3, 19, 4, 6, 7, 44, 13, 5, 2, 24, 14]. An efficient finite-element approach with an accurate treatment of the inextensibility condition can be used to find equilibria of free elastic rods [7] and self-avoiding rods [12, 13]. It can also be generalized to include twist contributions defined via torsion quantities [11]. We follow common conventions and refer to rods as *elastic curves* when twist contributions are omitted.

In this manuscript, a generalization of the existing scheme to calculate elasticae of *confined* elastic curves is proposed. Confinements of elastic structures arise on a variety of length scales, such as DNA plasmids or biopolymers inside a cell or chamber [17, 39]. The boundary of closely packed elastic sheets or a wire in a container can be modelled as confined elastic rods in two dimensions [22, 15]. A planar setting has been assessed in terms of phase-field modelling [23, 45]; a numerical scheme for thick elastic curves in containers is devised in [43].

We propose an approach that can be used for rods embedded in arbitrary dimensions confined to convex domains. For the mathematical modelling, we use a gradient flow to minimize the bending energy. The admissible rod configurations during the flow are restricted to a domain $D \subset \mathbb{R}^3$.

The task to unbend a rod inside D can be translated to minimizing E_{bend} among all

$$u \in \mathcal{A} \cap D, \quad \mathcal{A} = \{v \in H^2(I; \mathbb{R}^3) : |v'| = 1 \text{ a.e., } L_{\text{bc}}(v) = \ell_{\text{bc}}\}.$$

The bounded linear operator $L_{\text{bc}} : H^2(I; \mathbb{R}^3) \to \mathbb{R}^\ell$ realizes appropriate boundary conditions. We restrict our considerations to those subsets D that can be written as finite intersections of *simple quadratic confinements* D_r, $r = 1, 2, \ldots, R$, i.e.,

$$D = \cap_{r=1}^R D_r, \quad D_r = \{y \in \mathbb{R}^3 : |y|_{D_r}^2 = y \cdot G_{D_r} y \le 1\}$$

for symmetric positive semi-definite matrices $G_{D_r} \in \mathbb{R}^{3 \times 3}$. We call the finite intersection a *composite quadratic confinement*. For ease of presentation we often consider one set D_r and then omit the index r. Some basic simple quadratic confinements are the ball with radius R and $G_D = I_3/R^2$, the ellipsoid with radii R_1, R_2, R_3 and $(G_D)_{ij} = \delta_{ij}/R_i^2$, or the space between two parallel planes with distance $2R$ with normal vector n and $G_D = nn^t/R^2$. Boxes and finite cylinders can be constructed as composite quadratic confinements. In general, any simple or composite quadratic confinement is a convex, closed, and connected set.

We enforce the confinement via a potential approach, so a non-negative term is added to the bending energy whenever the curve violates the confining restrictions. We define a potential $V_D : \mathbb{R}^3 \to \mathbb{R}$ for a simple quadratic confinement D that vanishes in D and is strictly positive on $\mathbb{R}^3 \backslash D$ via

$$V_D(y) = \frac{1}{2} \left(|y|_D - 1 \right)_+^2 = \frac{1}{2} |y|_D^2 + \frac{1}{2} V_D^{\text{cv}}(y),$$

where the concave part V_D^{cv} is given by the continuous function

$$V_D^{\text{cv}}(y) = \begin{cases} -|y|_D^2, & \text{if } y \in D, \\ -2|y|_D + 1 & \text{else.} \end{cases}.$$

The potential is used to define a penalizing *confinement energy* functional

$$E_D[u] = \int_I |u(x)|_D^2 + V_D^{\text{cv}}(u(x)) \, \mathrm{d}x,$$

which is by the definition of the potential non-negative and zero if and only if the curve entirely lies within D. For a composite confinement defined via a family $(D_r)_{r=1,\ldots,R}$ of simple quadratic confinements we sum the corresponding confinement energies up, i.e.,

$$
(1) \qquad E_D[u] = \sum_{r=1}^{R} E_{D_r}[u], \quad V_D(y) = \sum_{r=1}^{R} V_{D_r}(y).
$$

We remark that translated domains and half-spaces, e.g., $D = \{y \in \mathbb{R}^3 : |y - y_D|_D^2 \leq 1\}$ and $D = \{y \in \mathbb{R}^3 : a_D \cdot y \leq 1\}$ can be similarly treated.

Given $\varepsilon > 0$, a curve $u_\varepsilon \in \mathcal{A}$ is called a *(approximately) confined elastica* if it is stationary for the functional

$$
E_\varepsilon[u] = E_{\mathrm{bend}}[u] + \frac{1}{2\varepsilon} E_D[u]
$$

in the set $\mathcal{A}$. If $V_D(u_\varepsilon) = 0$ almost everywhere on I, the rod is called *exactly confined elastica*. The parameter ε determines the steepness of the quadratic well potential and defines a length-scale for the penetration depth of the curve into the space outside of D.

Considering a simple quadratic confinement $D \subset \mathbb{R}^3$, we let $V_D \in C^1(\mathbb{R}^3; \mathbb{R})$ be the corresponding quadratic-well potential, and choose $\varepsilon > 0$. Trajectories $u \in H^1([0,T]; L^2(I; \mathbb{R}^3)) \cap L^\infty([0,T]; \mathcal{A})$ are defined by gradient flow evolutions. In particular, for an inner product $(\cdot, \cdot)_\star$ on $L^2(I; \mathbb{R}^3)$ and an initial configuration $u(0, x) = u_0(x)$, we define the temporal evolution as the solution of the time-dependent nonlinear system of partial differential equations

$$
(2) \qquad
\begin{aligned}
(\partial_t u, v)_\star + \kappa(u'', v'') &+ \varepsilon^{-1}(u, G_D v) \\
&= -(2\varepsilon)^{-1}(\nabla V_D^{\mathrm{cv}}(u), v) - (\lambda u', v')
\end{aligned}
$$

for test functions $v \in \mathcal{V}$ with a suitable set $\mathcal{V}$ and all $t \in [0, T]$. The function $\lambda \in L^1([0,T] \times I)$ is a Lagrange multiplier associated with the arc-length condition. Confined elasticae are stationary points for (2).

For time discretization, we use backward differential quotients. Let $\tau > 0$ be the fixed time-step and let $k \geq 0$ be a non-negative integer. We set $u^0 := u_0$ and define the time-step

$$
d_t u^{k+1} = \frac{u^{k+1} - u^k}{\tau}.
$$

The gradient flow system is evaluated implicitly except for the concave confinement energy, which is handled explicitly due to its non-linearity and anti-monotonicity, and the Lagrange multiplier term, which is treated semi-implicitly. We hence have

$$
(3) \qquad
\begin{aligned}
(d_t u^{k+1}, v)_\star + \kappa([u^{k+1}]'', v'') &+ \varepsilon^{-1}(u^{k+1}, G_D v) \\
&= -(2\varepsilon)^{-1}(\nabla V_D^{\mathrm{cv}}(u^k), v) - (\lambda^{k+1}[u^k]', v')
\end{aligned}
$$

for suitable test curves $v \in \mathcal{V}$. To ensure that the parametrization by arc-length is approximately preserved throughout the gradient flow, the constraint $|[u^k]'|^2 = 1$ is linearized. This yields the first order orthogonality condition

$$[u^k]' \cdot [d_t u^{k+1}]' = 0 \text{ on } I. \tag{4}$$

By imposing the same condition on test curves, i.e.,

$$[u^k]' \cdot v' = 0 \text{ on } I, \tag{5}$$

the Lagrange multiplier term disappears in (4). Given $u^0, u^1, \ldots, u^k \in H^2(I; \mathbb{R}^3)$, there are unique functions $d_t u^{k+1} \in H^2(I; \mathbb{R}^3)$ that solve the gradient flow equation (3) with all v satisfying (5) and $L_{\mathrm{bc}}[v] = 0$. This is a direct consequence of the Lax-Milgram lemma.

For numerical computations, we subdivide I into a partition $\mathcal{P}_h$ of maximal length h, which can be represented by the nodes $x_0 < x_1 < \ldots < x_N$. We use the space of piecewise cubic, globally continuously differentiable splines on $\mathcal{P}_h$ as a conforming subspace $V_h \subset H^2(I)$. On an interval $[x_i, x_{i+1}]$, these functions are entirely defined by the values and the derivatives at the endpoints. We also employ the space of piecewise linear, globally continuous finite element functions that are determined by the nodal values and denote the set by W_h. The corresponding interpolation operators are denoted as $\mathcal{I}_{3,h}$ and $\mathcal{I}_{1,h}$, respectively. We impose the orthogonality of $d_t u_h^{k+1}$ and u_h^k only at the nodes. The confinement quantities are evaluated by mass lumping, so only the values at the nodes are required

$$(v, w)_h := \int_I \mathcal{I}_{1,h}(v \cdot w) \, \mathrm{d}x.$$

In the nodal points, the concavity of V_D^{cv} is utilized to prove an energy monotonicity property.

The discrete admissible set is defined via

$$\mathcal{A}_h := \{u_h \in V_h^3 : |u_h'(x_i)|^2 = 1, \ i = 0, 1, \ldots, N, \ L_{\mathrm{bc}}[u_h] = \ell_{\mathrm{bc}}\},$$

and we write $u_h \in \mathcal{A}_h \cap D$ if $u_h(x_i) \in D$ for $i = 0, 1, \ldots, N$. The set of test functions relative to u_h is

$$\mathcal{F}_h[u_h] := \{v_h \in V_h^3 : u_h'(x_i) \cdot v_h'(x_i) = 0, \ i = 0, 1, \ldots, N, \ L_{\mathrm{bc}}[v_h] = 0\}.$$

We thus obtain the following fully practical numerical scheme to compute confined elasticae: Given $u_h^0 \in \mathcal{A}_h$ define $u_h^1, \ldots, u_h^k \in V_h^3$ by calculating $d_t u_h^{k+1} \in \mathcal{F}_h[u_h^k]$ such that

$$\begin{aligned} (d_t u_h^{k+1}, v_h)_\star + \kappa([u_h^k]'' + \tau[d_t u_h^{k+1}]'', v_h'') + \varepsilon^{-1}(u_h^k + \tau d_t u_h^{k+1}, G_D v_h)_h \\ = -(2\varepsilon)^{-1}(\nabla V_D^{\mathrm{cv}}(u_h^k), v_h)_h \end{aligned} \tag{6}$$

for all $v_h \in \mathcal{F}_h[u_h^k]$.

The remainder of this paper is structured into a first part proving the convergence of the proposed numerical scheme and into a second part that presents results of numerical experiments and describes confined elasticae

for closed rods in balls. The numerical simulations were done in the web application KNOTEVOLVE [9] which is accessible at `aam.uni-freiburg.de/knotevolve`.

2. CONVERGENCE RESULTS

In this section, we provide convergence results following ideas from [10]. The first result establishes the unconditional variational convergence of the discrete minimization problems to the continuous one defining confined elasticae. The following partial Γ convergence result relies on a regularity condition and is a consequence of conformity properties of the discrete model.

Proposition 2.1. *Define $E_h : H^2(I; \mathbb{R}^3) \to \mathbb{R} \cup \{+\infty\}$ via*

$$E_{h,\varepsilon}[u_h] = \frac{\kappa}{2} \int_I |u_h''|^2 \, \mathrm{d}x + \frac{1}{2\varepsilon} \int_I \mathcal{I}_{1,h} V_D(u_h) \, \mathrm{d}x$$

if $u_h \in \mathcal{A}_h$ and $E_h[u_h] = +\infty$ if $u_h \in H^2(I; \mathbb{R}^3) \setminus \mathcal{A}_h$. Analogously, let

$$E_{\mathrm{bend}}[u] = \frac{\kappa}{2} \int_I |u''|^2 \, \mathrm{d}x$$

for $u \in \mathcal{A} \cap D$ and $E_{\mathrm{bend}}[u] = +\infty$ if $u \in H^2(I; \mathbb{R}^3) \setminus \mathcal{A}$.
(i) For every sequence $(u_h)_{h>0} \subset H^2(I; \mathbb{R}^3)$ with weak limit $u \in H^2(I)$ we have $E_{\mathrm{bend}}[u] \leq \liminf_{(h,\varepsilon)\to 0} E_{h,\varepsilon}[u_h]$.
(ii) For every $u \in \mathcal{A} \cap D$ with $u \in H^3(I; \mathbb{R}^3)$ there exists a sequence $(u_h)_{h>0} \subset H^2(I; \mathbb{R}^3)$ such that $\lim_{(h,\varepsilon)\to 0} E_{h,\varepsilon}[u_h] = E_{\mathrm{bend}}[u]$.

Proof. Throughout this proof we write $h \to 0$ for a sequence $(h, \varepsilon) \to 0$.
(i) We consider a sequence $(u_h)_{h>0} \subset H^2(I; \mathbb{R}^3)$ and a limit $u \in H^2(I; \mathbb{R}^3)$ with $u_h \rightharpoonup u$ in $H^2(I; \mathbb{R}^3)$ as $h \to 0$. To show that $E[u] \leq \liminf_{h\to 0} E_{h,\varepsilon}[u_h]$ it suffices to consider the case that the bound is finite. Since $\mathcal{I}_{1,h} |u_h'|^2 = 1$ we find that

$$\big\| |u_h'|^2 - 1 \big\|_{L^2(I)} \leq ch \big\| (|u_h'|^2)' \big\|_{L^2(I)} \leq ch \|u_h''\|_{L^2(I)} \|u_h'\|_{L^\infty(I)},$$

which by embedding results implies that $|u'|^2 = 1$ in I. Similarly, since $\|\mathcal{I}_{1,h} V_D(u_h)\|_{L^1(I)} \to 0$ it follows that $u \in D$ in I. Since the bending energy is weakly lower semicontinuous and the potential term non-negative, we deduce the asserted inequality.
(ii) Given $u \in \mathcal{A} \cap D$ such that $u \in H^3(I; \mathbb{R}^3)$ we define $u_h = \mathcal{I}_{3,h} u$ and note that $u_h \to u$ in $H^2(I; \mathbb{R}^3)$ and $u_h(x_i) \in D$ as well as $|u_h'(x_i)| = 1$ for all $i = 0, 1, \ldots, N$, in particular $u_h \in \mathcal{A}_h$. This implies that $\lim_{h\to 0} E_{h,\varepsilon}[u_h] = E_{\mathrm{bend}}[u]$. $\square$

Remark 2.2. *The regularity condition can be avoided if a density result for inextensible confined curves in the spirit of [30] is available. Alternatively, a standard regularization of a given curve $u \in \mathcal{A} \cap D$ can be considered following [11, 14] which requires an appropriate scaling of the discretization and penalty parameters.*

The proposition implies the convergence of discrete (almost) minimizers provided that the boundary conditions imply a coercivity proper and exact minimizers are regular.

Corollary 2.3. *Assume that minimizers $u \in \mathcal{A} \cap D$ for E_{bend} satisfy $u \in H^3(I;\mathbb{R}^3)$, and that there exists $c > 0$ such that $\|v\|_{H^2(I)} \le c\|v''\|_{L^2(I)}$ for all $v \in H^2(I;\mathbb{R}^3)$ with $L_{\mathrm{bc}}[v] = 0$ or D is bounded. Then sequences of discrete almost minimizers for $E_{h,\varepsilon}$ accumulate weakly in $H^2(I;\mathbb{R}^3)$ at minimizers for E_{bend}.*

Our second convergence result concerns an estimate on the confinement violation.

Proposition 2.4. *Let $u_h \in \mathcal{A}_h$. Then we have that*

$$\|\mathcal{I}_{1,h}(|u_h|_D - 1)_+\|_{L^\infty(I)} \le c\varepsilon^{1/3}\big(E_{h,\varepsilon}[u_h]\big)^{1/3}.$$

Proof. The Gagliardo–Nirenberg inequality bounds the norm in $L^p(I)$ by the product of norms in $L^q(I)$ and $W^{1,r}(I)$ with exponents $1-\alpha$ and α such that $\frac{1}{p} + \frac{1}{q} = \alpha(1 - \frac{1}{r} + \frac{1}{q})$, cf. [34]. With $p = r = \infty, q = 2, \alpha = 1/3$ we have

$$\|\mathcal{I}_{1,h}(|u_h|_D-1)_+\|_{L^\infty(I)} \le c\|\mathcal{I}_{1,h}(|u_h|_D-1)_+\|_{L^2(I)}^{2/3}\|\mathcal{I}_{1,h}(|u_h|_D-1)_+\|_{W^{1,\infty}(I)}^{1/3}.$$

The $W^{1,\infty}$ norm can be uniformly bounded due to stability of the nodal interpolation operator in $W^{1,\infty}$ and the nodal constraints $|u_h'(x_i)|^2 = 1$, $i = 0, 1, \dots, N$. The term $(\varepsilon^{-1}\|\mathcal{I}_{1,h}(|u_h|_D - 1)_+\|_{L^2}^2)^{1/3}$ is bounded by the third root of the potential part of the discrete energy. $\qquad\square$

Remark 2.5. *A stronger estimate on the constraint violation can be derived if the solution u and the Lagrange multiplier λ are sufficiently regular, so that the Euler–Lagrange equations hold in strong form, i.e., $\kappa u^{(4)} + \varepsilon^{-1}\nabla V_D(u) = (\lambda u')'$, which implies $\|\nabla V_D(u)\|_{L^\infty(I)} = \mathcal{O}(\varepsilon)$, where $|\nabla V_D(y|$ is proportional to the distance of a point $y \in \mathbb{R}^3$ to the set D.*

Our third convergence result follows from the unconditional energy stability of the numerical scheme and states that the sequence of corrections $(d_t u_h^k)_{k=1,2,\dots}$ converges to zero as $k \to \infty$. Moreover, it provides a bound on the violation of the arclength constraint due to its linearized treatment.

Proposition 2.6. *The iterates $(u_h^k)_{k=0,1,\dots}$ of the scheme (6) satisfy*

$$E_{h,\varepsilon}[u_h^K] + \tau\sum_{k=1}^K \|d_t u_h^{k+1}\|_\star^2 \le E_{h,\varepsilon}[u_h^0],$$

for all $K \ge 0$, and, provided that $\|v\|_{L^\infty(I)} \le c_\star\|v\|_\star$,

$$\|\mathcal{I}_{1,h}|u_h'|^2 - 1\|_{L^\infty(I)} \le c_\star^2 \tau E_{h,\varepsilon}[u_h^0].$$

Proof. By concavity of V_D^{cv} we have that

$$V_D^{\mathrm{cv}}(u_h^k) + \nabla V_D^{\mathrm{cv}}(u_h^k) \cdot \big(u_h^{k+1} - u_h^k\big) \ge V_D^{\mathrm{cv}}(u_h^{k+1}).$$

This implies that by choosing $v_h = d_t u_h^{k+1}$ in (6) we have

$$\|d_t u_h^{k+1}\|^2 + d_t\left\{\frac{1}{2}\|[u_h^{k+1}]''\|^2 + \frac{1}{2\varepsilon}\int_I \mathcal{I}_h V_D(u_h^{k+1})\,\mathrm{d}x\right\} \le 0.$$

Multiplication by τ and summation over $k = 0, 1, \ldots, K-1$ yield the stability estimate. The orthogonality $[u_h^{k-1}]' \cdot [d_t u_h^k]'$ for $k = 1, 2, \ldots, K$ at the nodes leads to the relation

$$|[u_h^k]'|^2 = |[u_h^{k-1}]'|^2 + \tau^2 |[d_t u_h^k]'|^2.$$

Summing this identity over $k = 1, 2, \ldots, K$, noting $|[u_h^0]'|^2 = 1$ at the nodes, and including the energy stability prove the estimate. $\qquad\square$

3. Elasticae in balls and cylinders

Our numerical calculations are performed in Matlab and with the Knote-volve web application [9]. We consider closed elastic rods confined to balls and cylinders. The highly symmetric stationary configurations found for balls give rise to the following definition that provides a concise classification via two integer numbers. For the scalar product $(d_t u_h^{k+1}, v_h)_\star$, we use the L^2 inner product. The parameter values $\kappa = 10$ and $\varepsilon = 1/(10\kappa)$ are employed if not stated otherwise.

Definition 3.1. *An arclength parametrized curve is called a μ-circle if it is a μ-fold covered planar circle. It is called a μ-ν-clew if it shows a ν-fold symmetry around one axis running through the center of the ball. The integer μ is then defined as the winding number of u around the rotational axis.*

As an illustrative example of the gradient flow, we use a trefoil knot of length 31.9 that is confined to a ball of radius 4.6 with $h \approx 0.3$ and $\tau = 0.1h$. [1] Snapshots of the evolution are depicted in Figure 1. Also, the bending energy $\kappa\|[u_h^k]''\|^2/2$, the confinement energy $(2\varepsilon)^{-1}E_D[u_h^k]$ and the violation of arc-length parametrization $\|\mathcal{I}_{1,h}\{|[u_h^k]'|^2 - 1\}\|_{L^\infty}$ are visualized as a function of k.

First, the trefoil knot evolves into a double-covered circle. At some point, it unfolds into a bent lemniscate whose outermost points reach the surface of the ball. This configuration then moves to the left and starts to unfold into a buckled circle that runs close to the ball's surface. The final elastica is a 1-2-clew. The symmetry axis of the elastica, which is also depicted in Figure 1, is different from the symmetry axis of the initial curve. The local curvature of the 1-2-clew is periodic along the curve with periodicity 4. We generally observe that the curvature of a μ-ν-clew is 2ν-periodic.

A similar shape was previously also obtained for modelling semiflexible biopolymers in spherical domains that are slightly smaller than the flat circle of the same length, cf. [39]. The shape that we call 1-2-clew also arises

---

[1]The example can be run via `aam.uni-freiburg.de/knotevolve/torus-2-3-97?Rho=0&CnfmType=ellipsoid&CnfmRadius=4.6,4.6,4.6&tmax=30000&StepW=0.1`

when packing a thick rope of maximal length without self-penetration on the sphere [27].

When confining a rod of length L to balls of varying radii, a multitude of equilibrium configurations is observed. Examples are illustrated in Figure 2 where we used C_4 and C_5 symmetric initial configurations. Both, the symmetry number ν and the winding number μ depend on the symmetry of the initial configuration and on the ratio L/R. All elasticae run close to the ball's surface and slightly exceed the confining domain. With decreasing radius, either the winding number or the symmetry number are gradually increased by 2. This follows from an increasing number of self-intersections of the rod that always affect two of its segments. The gradient flow used to minimize the energy preserves certain symmetries. When starting with an even symmetry, the elastica is an odd-even-clew or an odd-circle as illustrated in Figure 2. An initially odd rotational symmetry in turn generally leads to even-odd-clews or even-circles. An exception is the transition from the 2-1-clew to the 1-2-clew as illustrated in the introductory example. This transition involves large deformations. When the radius of the ball is too small, the confinement is too restrictive for the curve to undergo such large transitions.

The unconfined elastica of a closed rod of length L is the circle of radius $r_L = L/(2\pi)$. The bending energy of this elastica is given by $E_L = \kappa L/(2r_L^2) = 2\kappa\pi^2/L$. To categorize the equilibrium configurations of closed rods that are confined to balls of radius R, we evaluate $(E_{\mathrm{bend}}/E_L)^{1/2}$ as a function of r_L/R. The first quantity measures the excess bending induced by the confinement, whereas the second quantity determines how many times too small the confining ball is compared to the unconfined elastica. We remark that for μ-fold covered circles, both quantities equal μ.

When starting with the four- and five-fold symmetric initial configurations, we observe two distinct families of the bending energy dependency on the ratio r_L/R. The result is shown in Figure 3. The elasticae in the five-fold symmetric case follow the pattern 1-circle, 1-2-clew, 3-2-clew, 3-circle, 3-4-clew, 5-4-clew, etc. for increasing r_L/R. In the four-fold symmetric case, we find (1-circle, 1-2-clew,) 2-1-clew, 2-circle, 2-3-clew, 4-3-clew, 4-circle, 4-5-clew, and so on. The first two are special as they involve a large deformation of the rod when transiting from the even-odd to odd-even. Both patterns are very regular and are expected to continue for larger r_L/R.

During the unfolding process, intermediate nearly stationary configurations are observed. These include a shape that could be called a 1-3-clew or multiply covered circles that are completely inside the ball. This can be seen in Figure 1: The initial rod evolves into a two-fold covered circle in the first place; later, the circle opens up. These configurations seem to be saddle-point structures as they are attractive with respect to the previous configuration, whereas there are adjacent configurations with smaller total energy. As the numerical representation of the rod cannot match those
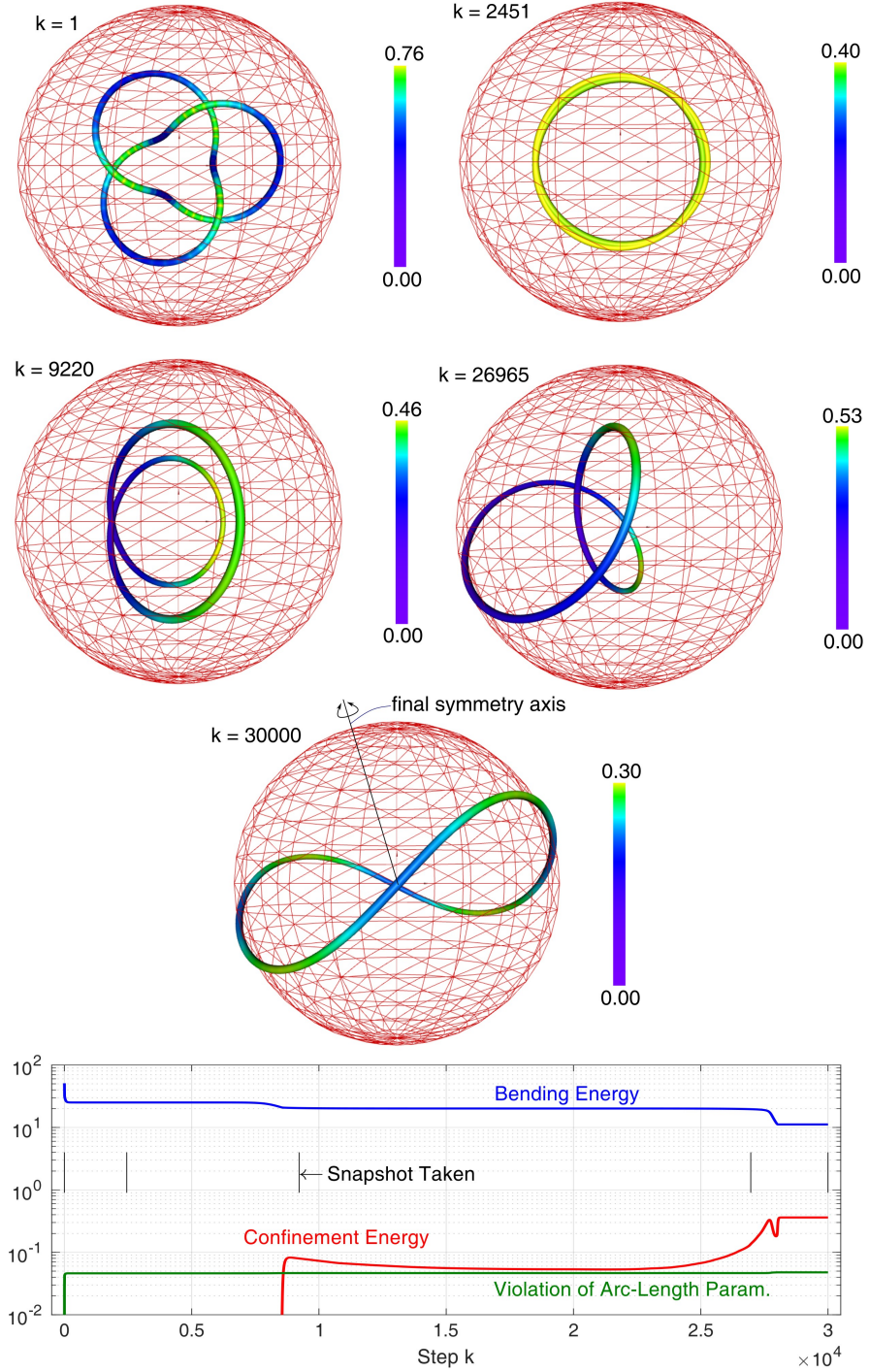
FIGURE 1. Evolution of a closed elastic curve in a ball of radius $R = 4.6$ to a 1-2-clew. The number k indicates the time steps, the color scheme represents local curvature. Confinement and total energy, and violation of arc-length parametrization are shown in the lower right panel.
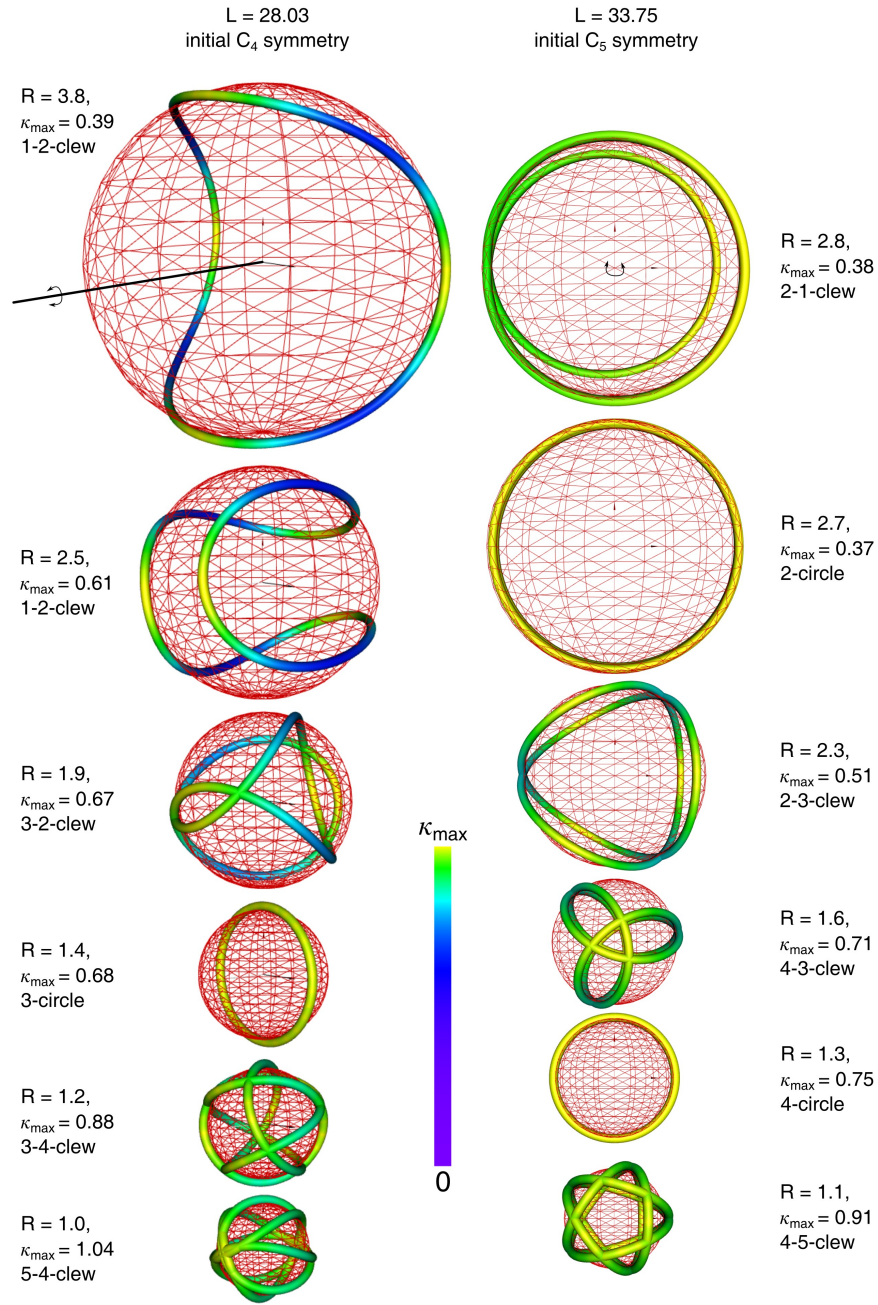
L = 28.03
initial C$_4$ symmetry

L = 33.75
initial C$_5$ symmetry

R = 3.8,
κ_{max} = 0.39
1-2-clew

R = 2.8,
κ_{max} = 0.38
2-1-clew

R = 2.5,
κ_{max} = 0.61
1-2-clew

R = 2.7,
κ_{max} = 0.37
2-circle

R = 1.9,
κ_{max} = 0.67
3-2-clew

R = 2.3,
κ_{max} = 0.51
2-3-clew

κ_{max}

R = 1.4,
κ_{max} = 0.68
3-circle

R = 1.6,
κ_{max} = 0.71
4-3-clew

R = 1.2,
κ_{max} = 0.88
3-4-clew

R = 1.3,
κ_{max} = 0.75
4-circle

0

R = 1.0,
κ_{max} = 1.04
5-4-clew

R = 1.1,
κ_{max} = 0.91
4-5-clew

FIGURE 2. Elastica shapes obtained for two different initial configurations (left and right column, respectively) and varying radii R. The color of the rod indicates the local curvature. The symmetry axis of the left column is indicated for the top configuration. In the right column, symmetry and view axes coincide.
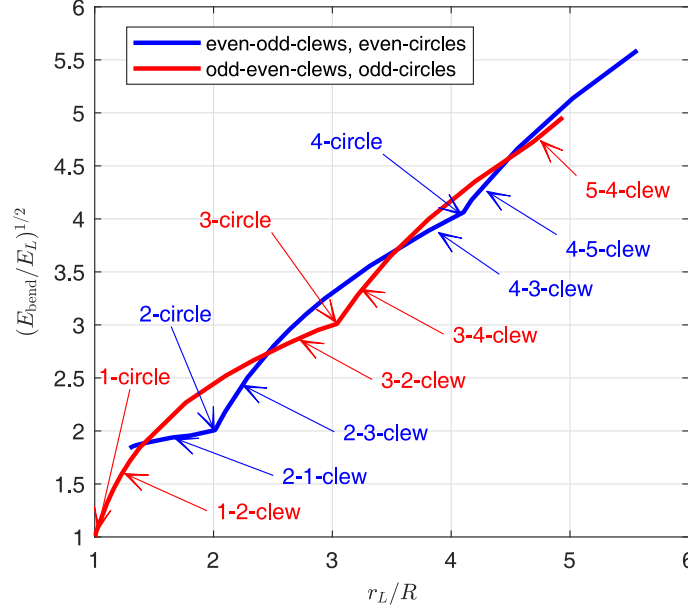
FIGURE 3. Normalized square root of the bending energy depending on the ratio r_L/R for the two observed elastica families

saddle-points perfectly, the rod exits those configurations after a certain number of steps.

For irregularly shaped initial rod configurations, the previously described elastica shapes are found as well. [2] Hence, the symmetry of the final shape can be attributed to solely the ratio r_L/R and to the question whether the initial configuration prefers the odd-even or even-odd elasticae family.

Conjecture 3.2. *Consider a rod of length L confined to a ball of radius R. Let $r_L = L/(2\pi)$ be the radius of the unconfined elastica and let $j \in \mathbf{N}$ be a positive integer with $j < r_L/R < j + 1$. Then there is a number $\xi(j) \in (0, 1)$ such that the globally least bent confined elastica is a j-$(j+1)$-clew if $r_L/R < j + \xi$. Else, the global optimizer is the $(j+1)$-j-clew. If $r_L/R < 1$, the flat 1-circle is an exactly confined elastica. In the cases where $r_L/R = j$ holds, the j-fold covered circle is the global elastica.*

The parameter ε can be understood as a length-scale of maximal penetration into the complement of D. The numerical results shown in Figure 4, indicate that
$$\max_{j=0,\ldots,N}(|u_h^k(x_j)|_D - 1)_+ = \mathcal{O}(\varepsilon).$$

---

[2]See for instance a knot with crossing number 10 relaxing into a 3-2-clew: `aam.uni-freiburg.de/knotevolve/10_053?Rho=0&StepW=0.1&CnfmType=ellipsoid&CnfmRadius=3,3,3`
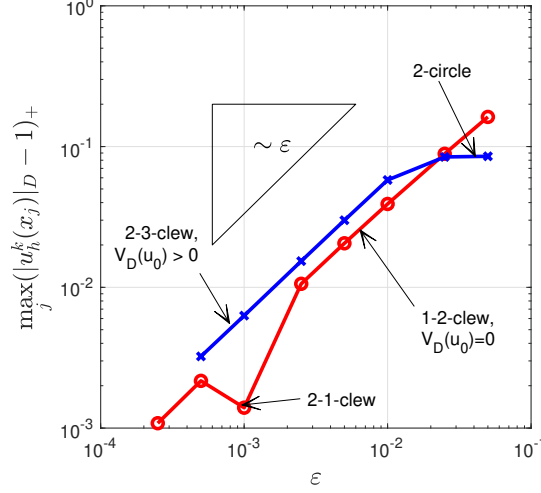
FIGURE 4. Maximal nodal penetration outside the confine-
ment domain depending on ε.

Thus, the maximal penetration decreases linearly with ε whilst not depend-
ing on whether the initial rod configuration lies inside D. This indicates
that the estimate as sketched in Remark 2.5 is valid in the case of spherical
confinements.

It can be observed that when varying ε for the same initial configuration
the final shape is not unique (cf. Figure 4): In the first example (dots in
Figure 4), mainly 1-2-clews were obtained as final shapes, but for one value
of ε, also a 2-1-clew could be observed. The second example that relaxed to
a 2-3-clew for sufficiently small ε (crosses in Figure 4), turned into a two-fold
covered circle if the confinement was too weak.

Interestingly, all elasticae for $r_L/R \geq 1$ lie on the surface of the ball up
to the penetration due to the finite potential. Brunnett and Crouch [16]
derived a differential equation for the geodesic curvature κ_g of the rod on
the sphere, i.e. the projection of the total curvature on the tangent plane in
each point:

$$\kappa_g'' + \frac{1}{2}\kappa_g^3 + C\kappa_g = 0.$$

Here, C is a constant consisting of the tension energy of the rod and the
sphere square curvature. This differential equation can be solved by the
Jacobi elliptic cosine function. The parameters of these functions must be
adjusted such that the curvature is periodic. When using the solution to
calculate the actual rod position, a nine-component ODE is solved, again
imposing periodicitiy. This raises the question whether the resulting config-
urations coincide with our experimentally observed μ-ν-clews and μ-circles,
thus leading to an analytic definition of our clews. For the μ-ν-clew, ν and μ
should arise when taking the periodic boundary conditions into account for

the geodesic curvature and the rod position, respectively. It would be also of analytic interest if all elasticae confined to balls are actually elasticae on the sphere. A proof would however go beyond the scope of this manuscript.

We close our discussion by experimentally investigating closed curves confined to cylinders of different heights and radii. [3] As shown in Figure 5, large cylinder heights apparently lead to flat configurations that resemble semi-circles connected by straight lines. If the cylinder is long enough, we assume that the true global elastica consists of two semi-circles connected by two straight lines. If height and diameter are equal, we observe a shape similar to a 4-3-clew (for height and diameter 6) or a 3-2-clew (for height and diameter 8). Other combinations of height and diameter reveal a large variety of optimal shapes. A concise classification as in the case of spherical confinement however is not obvious.

References

[1] A. Balaeff, L. Mahadevan, and K. Schulten. Modeling dna loops using the theory of elasticity. *Phys. Rev. E*, 73:031919, 3, Mar. 2006. DOI: `10.1103/PhysRevE.73.031919`.

[2] J. W. Barrett, H. Garcke, and R. Nürnberg. Finite element methods for fourth order axisymmetric geometric evolution equations. *J. Comput. Phys.*, 376:733–766, 2019. DOI: `10.1016/j.jcp.2018.10.006`.

[3] J. W. Barrett, H. Garcke, and R. Nürnberg. Numerical approximation of anisotropic geometric evolution equations in the plane. *IMA J. Numer. Anal.*, 28(2):292–330, 2008. DOI: `10.1093/imanum/drm013`.

[4] J. W. Barrett, H. Garcke, and R. Nürnberg. Numerical approximation of gradient flows for closed curves in $\mathbb{R}^d$. *IMA J. Numer. Anal.*, 30(1):4–60, 2010. DOI: `10.1093/imanum/drp005`.

[5] J. W. Barrett, H. Garcke, and R. Nürnberg. Stable discretizations of elastic flow in Riemannian manifolds. *SIAM J. Numer. Anal.*, 57(4):1987–2018, 2019. DOI: `10.1137/18M1227111`.

[6] J. W. Barrett, H. Garcke, and R. Nürnberg. The approximation of planar curve evolutions by stable fully implicit finite element schemes that equidistribute. *Numer. Methods Partial Differential Equations*, 27(1):1–30, 2011. DOI: `10.1002/num.20637`.

[7] S. Bartels. A simple scheme for the approximation of the elastic flow of inextensible curves. *IMA J. Numer. Anal.*, 33(4):1115–1125, 2013. DOI: `10.1093/imanum/drs041`.

[8] S. Bartels. Finite element simulation of nonlinear bending models for thin elastic rods and plates. In *Geometric partial differential equations. Part I*. Volume 21, Handb. Numer. Anal. Pages 221–273. Elsevier/North-Holland, Amsterdam, 2020.

[9] S. Bartels, P. Falk, and P. Weyer. KNOTEVOLVE – a tool for relaxing knots and inextensible curves, 2020. `https://aam.uni-freiburg.de/knotevolve/`.

[10] S. Bartels and C. Palus. Stable gradient flow discretizations for simulating bilayer plate bending with isometry and obstacle constraints. *IMA Journal of Numerical Analysis*, July 2021. DOI: `10.1093/imanum/drab050`. eprint: `https://academic.oup.com/imajna/advance-article-pdf/doi/10.1093/imanum/drab050/38894644/drab050.pdf`. drab050.

[11] S. Bartels and P. Reiter. Numerical solution of a bending-torsion model for elastic rods. *Numer. Math.*, 146(4):661–697, 2020. DOI: `10.1007/s00211-020-01156-6`.

---

[3]See for instance `aam.uni-freiburg.de/knotevolve/torus-1-13-100?Rho=0&StepW=0.2&CnfmType=cylinder-z&CnfmRadius=3,3,3&tmax=200000`
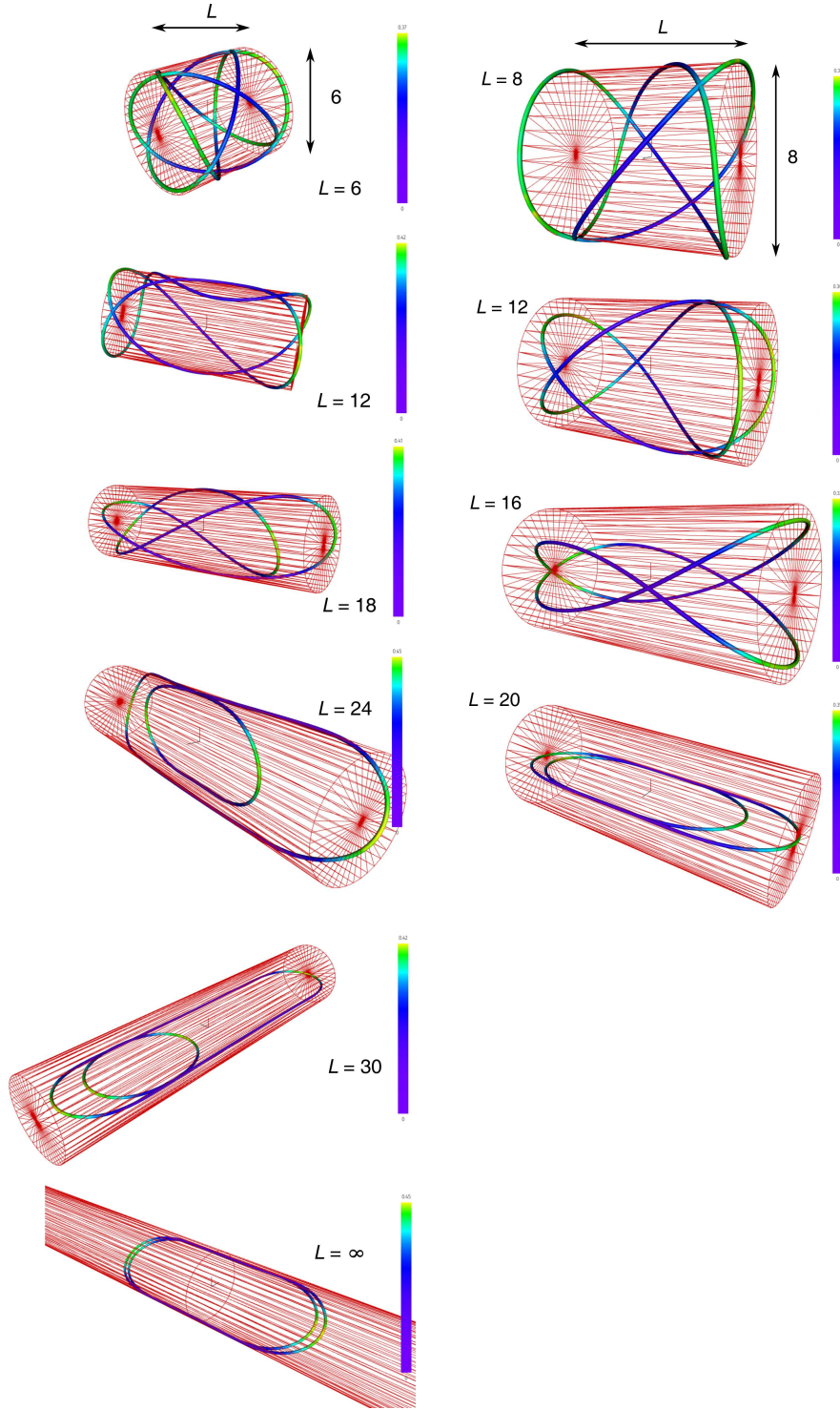
FIGURE 5. Stationary closed curves in cylindrical domains
with radii $R = 3$ (left) and $R = 4$ (right) and different heights
(increasing from top to bottom).

[12] S. Bartels and P. Reiter. Stability of a simple scheme for the approximation of elastic knots and self-avoiding inextensible curves. *Math. Comp.*, 90(330):1499–1526, 2021. DOI: `10.1090/mcom/3633`.

[13] S. Bartels, P. Reiter, and J. Riege. A simple scheme for the approximation of self-avoiding inextensible curves. *IMA J. Numer. Anal.*, 38(2):543–565, 2018. DOI: `10.1093/imanum/drx021`.

[14] A. Bonito, D. Guignard, R. H. Nochetto, and S. Yang. LDG approximation of large deformations of prestrained plates. *J. Comput. Phys.*, 448:Paper No. 110719, 27, 2022. DOI: `10.1016/j.jcp.2021.110719`.

[15] L. Boué, M. Adda-Bedia, A. Boudaoud, D. Cassani, Y. Couder, A. Eddi, and M. Trejo. Spiral patterns in the packing of flexible structures. *Phys. Rev. Lett.*, 97:166104, 16, Oct. 2006. DOI: `10.1103/PhysRevLett.97.166104`.

[16] G. Brunnett and P. E. Crouch. Elastic curves on the sphere. *Adv. Comput. Math.*, 2(1):23–40, 1994. DOI: `10.1007/BF02519034`.

[17] M. C. Choi, C. D. Santangelo, O. Pelletier, J. H. Kim, S. Y. Kwon, Z. Wen, Y. Li, P. A. Pincus, C. R. Safinya, and M. W. Kim. Direct observation of biaxial confinement of a semiflexible filament in a channel. *Macromolecules*, 38(23):9882–9884, 2005. DOI: `10.1021/ma051348n`. eprint: `https://doi.org/10.1021/ma051348n`.

[18] A. Dall'Acqua, C.-C. Lin, and P. Pozzi. Evolution of open elastic curves in $\mathbb{R}^n$ subject to fixed length and natural boundary conditions. *Analysis (Berlin)*, 34(2):209–222, 2014. DOI: `10.1515/anly-2014-1249`.

[19] K. Deckelnick and G. Dziuk. Error analysis for the elastic flow of parametrized curves. *Math. Comp.*, 78(266):645–671, 2009. DOI: `10.1090/S0025-5718-08-02176-5`.

[20] K. Deckelnick, G. Dziuk, and C. M. Elliott. Computation of geometric partial differential equations and mean curvature flow. *Acta Numer.*, 14:139–232, 2005. DOI: `10.1017/S0962492904000224`.

[21] E. H. Dill. Kirchhoff's theory of rods. *Arch. Hist. Exact Sci.*, 44(1):1–23, 1992. DOI: `10.1007/BF00379680`.

[22] C. C. Donato, M. A. F. Gomes, and R. E. de Souza. Scaling properties in the packing of crumpled wires. *Phys. Rev. E*, 67:026110, 2, Feb. 2003. DOI: `10.1103/PhysRevE.67.026110`.

[23] P. W. Dondl, L. Mugnai, and M. Röger. Confined elastic curves. *SIAM J. Appl. Math.*, 71(6):2205–2226, 2011. DOI: `10.1137/100805339`.

[24] W. Dörfler and R. Nürnberg. Discrete gradient flows for general curvature energies. *SIAM J. Sci. Comput.*, 41(3):A2012–A2036, 2019. DOI: `10.1137/18M122844X`.

[25] G. Dziuk, E. Kuwert, and R. Schätzle. Evolution of elastic curves in $\mathbb{R}^n$: existence and computation. *SIAM J. Math. Anal.*, 33(5):1228–1245, 2002. DOI: `10.1137/S0036141001383709`.

[26] P. B. Furrer, R. S. Manning, and J. H. Maddocks. DNA rings with multiple energy minima. *Biophysical Journal*, 79(1):116–136, 2000. DOI: `https://doi.org/10.1016/S0006-3495(00)76277-1`.

[27] H. Gerlach and H. von der Mosel. What are the longest ropes on the unit sphere? *Arch. Ration. Mech. Anal.*, 201(1):303–342, 2011. DOI: `10.1007/s00205-010-0390-y`.

[28] A. E. Green, N. Laws, and P. M. Naghdi. A linear theory of straight elastic rods. *Arch. Rational Mech. Anal.*, 25(4):285–298, 1967. DOI: `10.1007/BF00250931`.

[29] M. Grothaus and N. Marheineke. On a nonlinear partial differential algebraic system arising in the technical textile industry: analysis and numerics. *IMA J. Numer. Anal.*, 36(4):1783–1803, 2016. DOI: `10.1093/imanum/drv056`.

[30] P. Hornung. Deformation of framed curves with boundary conditions. *Calc. Var. Partial Differential Equations*, 60(3):Paper No. 87, 26, 2021. DOI: `10.1007/s00526-021-01980-0`.

[31] G. Kirchhoff. Ueber das Gleichgewicht und die Bewegung eines unendlich dünnen elastischen Stabes. *J. Reine Angew. Math.*, 56:285–313, 1859. DOI: `10.1515/crll.1859.56.285`.

[32] J. Langer and D. A. Singer. Curve straightening and a minimax argument for closed elastic curves. *Topology*, 24(1):75–88, 1985. DOI: `10.1016/0040-9383(85)90046-1`.

[33] J. Langer and D. A. Singer. Knotted elastic curves in $\mathbb{R}^3$. *J. London Math. Soc. (2)*, 30(3):512–520, 1984. DOI: `10.1112/jlms/s2-30.3.512`.

[34] G. Leoni. *A first course in Sobolev spaces*, volume 181 of *Graduate Studies in Mathematics*. American Mathematical Society, Providence, RI, second edition, 2017, pages xxii+734. DOI: `10.1090/gsm/181`.

[35] A. Manhart, D. Oelz, C. Schmeiser, and N. Sfakianakis. An extended filament based lamellipodium model produces various moving cell shapes in the presence of chemotactic signals. *J. Theoret. Biol.*, 382:244–258, 2015. DOI: `10.1016/j.jtbi.2015.06.044`.

[36] M. G. Mora and S. Müller. Derivation of the nonlinear bending-torsion theory for inextensible rods by Γ-convergence. *Calc. Var. Partial Differential Equations*, 18(3):287–305, 2003. DOI: `10.1007/s00526-003-0204-2`.

[37] C. G. Mulcahy, T. Su, N. Wicks, and P. M. Reis. Extending the Reach of a Rod Injected Into a Cylinder Through Axial Rotation. *Journal of Applied Mechanics*, 83(5), Feb. 2016. DOI: `10.1115/1.4032500`. eprint: `https://asmedigitalcollection.asme.org/appliedmechanics/article-pdf/83/5/051003/6082462/jam\_083\_05\_051003.pdf`. 051003.

[38] D. B. Öelz. On the curve straightening flow of inextensible, open, planar curves. *SeMA J.*, (54):5–24, 2011. DOI: `10.1007/bf03322585`.

[39] K. Ostermeir, K. Alim, and E. Frey. Buckling of stiff polymer rings in weak spherical confinement. *Phys. Rev. E*, 81:061802, 6, June 2010. DOI: `10.1103/PhysRevE.81.061802`.

[40] T. Ranner. A stable finite element method for low inertia undulatory locomotion in three dimensions. *Appl. Numer. Math.*, 156:422–445, 2020. DOI: `10.1016/j.apnum.2020.05.009`.

[41] P. Reiter and H. Schumacher. Sobolev gradients for the Möbius energy. *Arch. Ration. Mech. Anal.*, 242(2):701–746, 2021. DOI: `10.1007/s00205-021-01680-1`.

[42] Y. Shi and J. E. Hearst. The Kirchhoff elastic rod, the nonlinear Schrödinger equation, and DNA supercoiling. *The Journal of Chemical Physics*, 101(6):5186–5200, 1994. DOI: `10.1063/1.468506`. eprint: `https://doi.org/10.1063/1.468506`.

[43] S. Walker. A descent scheme for thick elastic curves with self-contact and container constraints. *Preprint*, 2021.

[44] S. W. Walker. Shape optimization of self-avoiding curves. *J. Comput. Phys.*, 311:275–298, 2016. DOI: `10.1016/j.jcp.2016.02.011`.

[45] S. Wojtowytsch. Confined elasticae and the buckling of cylindrical shells. *Adv. Calc. Var.*, 14(4):555–587, 2021. DOI: `10.1515/acv-2019-0033`.

Email address: `bartels@mathematik.uni-freiburg.de`

ABTEILUNG FÜR ANGEWANDTE MATHEMATIK, ALBERT-LUDWIGS-UNIVERSITÄT FREIBURG, HERMANN-HERDER-STR. 10, 79104 FREIBURG I. BR., GERMANY